Journal of Catalysis **208,** 187–196 (2002)
doi:10.1006/jcat.2002.3564, available online at http://www.idealibrary.com on IDEAL®

Phosphorus-Doped Molybdenum Oxynitrides and Oxygen-Modified Molybdenum Carbides: Synthesis, Characterization, and Determination of Turnover Rates for Propene Hydrogenation

P. Perez-Romo,* C. Potvin,* J.-M. Manoli,*,[1] M. M. Chehimi,† and G. Djéga-Mariadassou*

**Laboratoire Réactivité de Surface, Université Pierre et Marie Curie, CNRS UMR 7609, Case 178, 4 place Jussieu, 75252 Paris Cedex 05, France; and †ITODYS, UPRESA 7036, Université Denis Diderot, 1 rue Guy de la Brosse, 75005 Paris, France*

Received November 16, 2001; revised February 14, 2002; accepted February 14, 2002

The effect of phosphorus on molybdenum oxynitrides and oxygen-modified carbides has been studied. Phosphorus was introduced via heteropolyanions. Catalysts were characterized by elemental analysis, X-ray diffraction, N_2 BET surface area, CO chemisorption, and X-ray photoelectron spectroscopy (XPS). XPS measurements show higher concentrations of lower Mo oxidation states on P addition to molybdenum oxynitrides. Two types of phosphorus were revealed by XPS spectra: phosphatelike at about 134 eV, and phosphide at 130 eV. Propene hydrogenation was used to probe the activity of the doped materials. Reactivity experiments over P-containing oxynitrides and oxygen-modified carbides show enhanced hydrogenating properties, in particular for the oxynitride materials. Turnover rate was studied as a function of P content.

Key Words: **catalysts; synthesis; characterization; molybdenum oxynitride; oxygen-modified molybdenum carbide; heteropolyanion precursor; phosphorus; hydrogenation.**

INTRODUCTION

In recent years there has been a growing interest in the study of the properties of early transition metal nitrides or carbides, which are active in several reactions traditionally catalyzed by noble metals (1–4). These materials often demonstrate advantages over their parent metals in activity, selectivity, and resistance to poisoning (5).

Phosphorus in the form of phosphate is frequently added to the solution of the metal salts to be impregnated, in order to improve the solubility, to enhance the active-phase thermal stability, or to modify the acidic sites of supported catalysts. In the past two decades, phosphorus has been especially incorporated into *in situ* sulfidated $NiMo/Al_2O_3$ hydrodenitrogenation (HDN) catalysts, a substantial promotional effect of phosphorus in such catalysts in HDN having been demonstrated (6, 7).

Indole HDN and benzothiophene hydrodesulfurization (HDS) were significantly increased by adding phosphorus to unsupported molybdenum nitrides (8, 9). Hydrogenation properties of tungsten oxynitrides (10) are enhanced when phosphorus is present. Isomerization of *n*-heptane with P-containing molybdenum oxynitride is highly selective, the main products always consisting of mono- and dimethyl isomers (11, 12). New catalysts with added P on alumina-supported molybdenum carbides were prepared by Oyama and coworkers (13). They are more active in the hydroprocessing of model liquid compounds than is $NiMoS/Al_2O_3$ and are sulfur tolerant. Novel phosphorus-doped alumina-supported molybdenum and tungsten carbides were tested in high-pressure (4 MPa) reactions. Tetralin hydrogenation was doubled (14) and 4,6-dimethyldibenzothiophene HDS was significantly enhanced (15, 16).

Phosphorus can be added to the oxide form of the nitride or carbide precursor as a separate salt or as a polyanionic compound together with transition metals (10, 11, 17). This method has the advantage of associating all elements in the same chemical unit. In the present work the synthesis and characterization of molybdenum nitrides and carbides are reported. The catalysts were synthesized from various heteropolyanions with different P/Mo ratios (from 0 to 0.4) by the temperature-programmed reaction method, then tested in propene hydrogenation. Elemental analysis, CO chemisorption, X-ray diffraction (XRD), BET surface area, and X-ray photoelectron spectroscopic (XPS) measurements were used to characterize the materials.

EXPERIMENTAL

Materials

Heteropolyanions with P/Mo atomic ratios ranging from 0 to 0.4 were purchased [$(NH_4)_6Mo_7O_{24},4H_2O$ with P/Mo = 0 and $H_3PMo_{12}O_{40},xH_2O$ with P/Mo = 0.08, Acros] or synthesized [$(NH_4)_6P_2Mo_{18}O_{62},xH_2O$ with

[1] To whom correspondence should be addressed. Fax: +33 (0)1 44 27 60 33. E-mail: jmm@ccr.jussieu.fr.

0021-9517/02 $35.00

P/Mo = 0.11 and $(NH_4)_6P_2Mo_5O_{23},xH_2O$ with P/Mo = 0.4] and used as precursors.

Reactant gases were ammonia (99.5%), methane (99.90%), and hydrogen (99.995%). For catalyst tests, propene, oxygen, helium, and argon (all 99.995%) and hydrogen purified by passing through an oxygen trap were used. All gases were supplied by Air Liquide.

Catalyst Preparation

Molybdenum oxynitrides and oxygen-modified carbides were prepared by temperature-programmed reaction (TPR) using a modification of the procedures described elsewhere (1). This method was also used by Li and Lee (8, 9) starting from $H_3PMo_{12}O_{40},xH_2O$ to synthesize P-doped molybdenum nitrides and carbides. Typical oxynitride syntheses were divided into two steps. First, the temperature of the precursors was raised quickly (heating rate, 120 K h^{-1}) from room temperature (RT) to 623 K in flowing NH_3 [volume hourly space velocity (VHSV), 15000 h^{-1}]. The materials were then nitrided using a lower linear heating rate (30 K h^{-1}) from 623 K to a variable final value (T_f = 973 K for the ammonium heptamolybdate precursor and 753 K for the others). The samples were held at T_f for 0.5 h for the ammonium heptamolybdate precursor and 4 h for the phosphorus-containing precursors. After rapid cooling to RT, the ammonia flow was switched to a O_2/Ar mixture (1% v/v) for a passivation step (10 L h^{-1} for 1 h).

Oxygen-modified molybdenum carbides were synthesized via a TPR between the precursors and a CH_4/H_2 mixture (30% v/v) with a VHSV of 7000 h^{-1}. The temperature was brought rapidly from RT to 650 K, then raised linearly (60 K h^{-1}) to 973 K and held at this temperature for 1 h. The gas mixture was then switched to H_2 and the sample cooled rapidly to RT. The sample was passivated with O_2/Ar (1% v/v, 10 L h^{-1} for 1 h).

Characterization

A gas chromatograph (GC) using a thermal conductivity detector and an automatic injection valve was used to analyze the gas at the outlet of the preparation reactor. Nitrogen, hydrogen, and ammonia were separated on a 1 m × 1/8 in. Porapak Q (Alltech) column at 350 K with helium as carrier gas. Methane and water were separated on a 0.9 m × 1/8 in. Porapak N (Alltech) at 373 K. A two-pen recorder was used to follow the progress of nitridation or carburization as a function of temperature.

Before elemental BET and XPS characterizations, all samples were pretreated with flowing hydrogen in a quartz reactor at 723 K (for oxynitrides with phosphorus) and 773 K (for oxynitrides without phosphorus and for all oxygen-modified carbides) for 4 h. They were then treated at 673 K under vacuum for 1 h and finally sealed in glass tubes. Elemental analyses were performed by the Service Central d'Analyse du Centre National de la Recherche Scientifique (Vernaison, France).

Specific surface areas (S_g) were determined by the N_2 BET method on a Micromeritics ASAP 2010 adsorption analyser. The samples treated as described above were degassed under vacuum for 4 h on the Micromeritics unit prior to measurement.

A Siemens D500 automatic diffractometer with a monochromated Cu K_α source was used to determine the XRD patterns of the solid phases. The analysis included crystallite size estimation from line broadening. The average crystallite size was calculated using the Scherrer formula (18): $D_{hkl} = 0.9\lambda/B\cos\theta$, where λ is the wavelength of the radiation, B the corrected peak width, and θ the Bragg angle of the peak.

The selective chemisorption of CO was used to titrate active metallic sites before runs and was performed by a pulse technique at 293 K. A known volume of CO controlled by an automatic valve was passed through a quartz reactor containing the material (0.3 g), with He being used as carrier gas. A thermal conductivity detector detected the remaining nonadsorbed CO at the outlet of the reactor. Hence, the consumption of CO was determined and the amount of CO chemisorbed by the sample deduced. Samples of molybdenum oxynitrides or oxygen-modified molybdenum carbides were first treated with flowing hydrogen in a quartz reactor at 723 K for 4 h, purged in flowing helium for 0.5 h, and then quenched at 293 K.

X-Ray Photoelectron Spectroscopy

X-ray photoelectron spectra were measured using a Surface Science Instrument, SSX 100 spectrometer with a monochromated Al K_α source ($h\nu$ = 1486.6 eV), a hemispherical electron analyzer, and a multichannel detector. Sealed glass tubes were opened in a glove box (dry argon) connected to the fast entry lock of the XPS machine. Materials were transferred to the sample holder without exposure to air. Samples were then outgassed in the fast entry lock before transfer to the analysis chamber. The vacuum during the measurements was typically 5×10^{-9} Torr and the data were collected in separate regions with acquisition times ranging from 5 to 10 s per spectral point. The C 1s peak of adventitious hydrocarbon (binding energy = 284.6 eV) was taken as reference in calculating binding energies and accounting for the charging effect. Experimental peaks were decomposed into components (90% Gaussian, 10% Lorentzian) using a nonlinear least-squares fitting algorithm and a Shirley baseline. To reconstruct molybdenum levels, parameter constraints were imposed. A splitting energy of 3.2 eV and an intensity ratio $I(Mo\,3d_{5/2})/I(Mo\,3d_{3/2}) = 3/2$ were used for the $Mo\,3d_{5/2}$–$Mo\,3d_{3/2}$ doublet. For the $Mo\,3p_{3/2}$–$Mo\,3p_{1/2}$ doublet a splitting energy of 17.5 eV and an intensity ratio $I(Mo\,3p_{3/2})/I(Mo\,3p_{1/2}) = 2$ were used. The surface composition (in

atom percent) of the various samples was determined by considering the integrated peaks of C 1s, N 1s, O 1s, Mo 3d, and P 2p using their respective experimental sensitivity factors (19). Binding energies were reproducible to within ±0.2 eV.

Propene Hydrogenation

Following Burwell (20) propene hydrogenation (a structure-insensitive reaction) was chosen as a model reaction to determine the hydrogenation properties of materials at atmospheric pressure. The passivated materials are nearly inactive in benzene hydrogenation at atmospheric pressure in the temperature range where 100% conversion is thermodynamically allowed. Propene hydrogenation presents a broader temperature range for comparing our materials.

The reaction was carried out in a flow reactor at 250 K (for oxygen-modified carbides) or 353 or 383 K (for oxynitrides), depending of the activity of the catalyst. The gas mixture (the H_2/C_3H_6 molar ratio was fixed at 6.7 and the total flow rate at 6.9 L h^{-1}) was fed into a Pyrex reactor loaded with the catalytic sample on a sintered glass disk (1 cm in diameter). The effluent composition was analyzed with a HP 5890 series II gas chromatograph equipped with a KCl-modified Al_2O_3 capillary column and a flame ionization detector. The only product observed was propane. Prior to each run, passivated catalysts were pretreated *in situ* at 723 K (for oxynitrides containing phosphorus) and 773 K (for oxynitrides without phosphorus and for all oxygen-modified carbides) in flowing hydrogen H_2 (0.72 L h^{-1}) for 4 h. The catalyst weight was chosen in order to obtain a conversion lower than 10%, allowing the assumption of a pseudo-zeroth order for propene. The reciprocal value of the conversion τ versus time of run t was used to determine the initial conversion τ_0 by extrapolation to zero time: $1/\tau = 1/\tau_0 + \kappa$ where κ is an empirical deactivation constant (21). The propene hydrogenation rate is expressed as turnover rate (TOR), defined as the number of propene molecules converted to propane per CO-titrated surface metal atom per second.

RESULTS AND DISCUSSION

Ammonia Decomposition and Methane Consumption during Preparation: TPR Experiments

Molybdenum nitrides. Previous work (1, 2, 22, 23) has shown that the properties of molybdenum nitrides are strongly dependent on the synthesis conditions, such as the ramping rate of preparation temperature, the space velocity (VHSV) of reactive gases, and the final temperature of TPR, as well as the time during which the sample is exposed at this temperature.

The formation of both face-centered cubic (fcc) γ-Mo_2N and hexagonal δ-MoN by nitriding molybdenum oxides has been reported. Our first aim was to find the conditions necessary to produce a pure γ-Mo_2N phase with high surface area. Recent work has shown that δ-MoN is not a catalyst for *n*-heptane isomerization (at 623 K and atmospheric pressure) (24) or toluene hydrogenation (at 673 K and 5 MPa) (25). During temperature-programmed nitridation the gas-phase concentrations of NH_3, N_2, and H_2 were monitored by GC. Decomposition of ammonia began between 623 and 653 K for all precursors and it was evident that all the materials with different P/Mo ratios followed the same reduction route. Therefore, a higher heating rate was employed during the first heating stage and a lower rate in a second step in order to avoid sintering the intermediates during the nitridation stage. It has been reported (2) that high space velocities result in large surface areas and favor the elimination of water (hydrothermal sintering) formed as a product of the reaction.

Ammonium heptamolybdate reacts with ammonia to form a mixture of nitride phases (γ-Mo_2N and δ-MoN). The Mo_2N/MoN ratio depends on the heating rate and on the final reaction temperature. This is shown by comparing the (202) XRD peak intensity of δ-MoN with that of the (200) peak of γ-Mo_2N. The best compromise (highest specific surface area, absence of δ-MoN) is obtained for a VHSV of 15000 h^{-1} and a final temperature of 973 K. For phosphorus-containing precursors, a pure γ-Mo_2N with the highest specific surface area is obtained at lower temperature (753 K) with the same VHSV. The molybdenum nitride synthesized from the precursor with a P/Mo ratio of 0.4 gives a small surface area (about 1 m^2) and was not further considered.

Molybdenum carbides. The carburization of the various precursor samples, conducted in a flow of CH_4/H_2 (30% v/v), was monitored by analyzing the consumption of methane and the formation of water. It was found that no changes occurred in the materials below 650 K, so the temperature program consists of two steps. Following rapid heating to 650 K in about 2 h, samples were further heated slowly to the final temperature (1023 K) with a linear ramping rate of 60 K h^{-1} and with a VHSV of 7000 h^{-1}. Figure 1 shows a typical TPR profile for the synthesis process. We observe for ammonium heptamolybdate four peaks for water formation and two methane consumption peaks. The first CH_4 consumption peak occurs almost simultaneously with the third stage of water production and corresponds to the carburization-reduction process (17, 26–28).

Carburization begins at 733 K and is complete at 973 K; the second CH_4 consumption is attributed to polymeric carbon (27). In contrast, for all the phosphorus-containing precursors only one methane consumption peak is observed, beginning and ending at a lower temperature than that required for ammonium heptamolybdate (except for the precursor with P/Mo = 0.4). No polymeric carbon is formed. Thus all the materials are carburized in the temperature

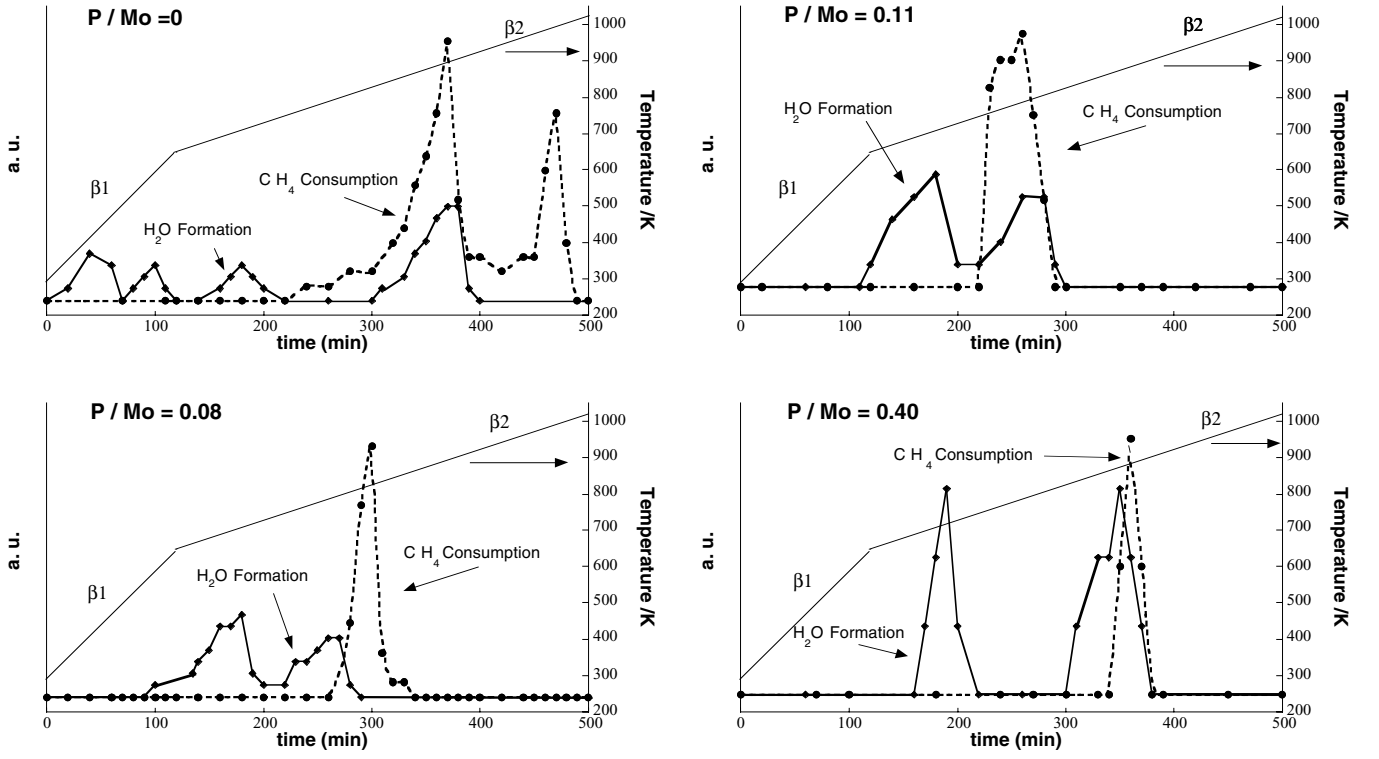

FIG. 1. TPR profiles for heteropolyanion precursors with P/Mo = 0, P/Mo = 0.08, P/Mo = 0.11, and P/Mo = 0.40 in flowing 30% v/v CH_4/H_2. Temperature versus time schedules used are noted β_1 (300 K h^{-1}) or β_2 (60 K h^{-1}).

range 730–973 K. The formation of a pure hexagonal close-packed (hcp) structure of β-Mo_2C was confirmed by XRD at the end of the TPR.

Influence of Phosphorus on XRD of Materials

The elemental analyses results (Table 1) for phosphorus-doped molybdenum nitrides reveal oxygen in all cases, with a metal/(N + O) ratio ranging from 0.48 to 0.84, which is lower than 2, the metal/N ratio required by the theoretical formula Mo_2N. We present the chemical formulas of these materials as $Mo_2N_xO_y$ or $Mo_2N_xO_yP_z$ and refer to them as oxynitrides.

TABLE 1

Physical Properties of Molybdenum Oxynitrides and Oxygen-Modified Carbides

Precursor	P/Mo ratio	Chemical analysis formula	Surface area, S_g (m^2 g^{-1})	Crystallite size, D_c (nm)
Oxynitrides				
$(NH_4)_6Mo_7O_{24}$	0	$Mo_2N_{2.7}O_{1.46}$	160	7.6
$H_3PMo_{12}O_{40}$	0.08	$Mo_2N_{2.82}O_{1.34}P_{0.2}$	52	2.0
$(NH_4)_6P_2Mo_{18}O_{62}$	0.11	$Mo_2N_{2.86}O_{0.82}P_{0.24}$	77	2.4
$(NH_4)_6P_2Mo_5O_{23}$	0.4	$Mo_2N_{1.08}O_{1.28}P_{0.82}$	<1	1.2
Oxygen-modified carbides				
$(NH_4)_6Mo_7O_{24}$	0	$Mo_2C_{1.46}O_{0.08}$	45	11.3
$H_3PMo_{12}O_{40}$	0.08	$Mo_2C_{0.9}O_{0.46}P_{0.16}$	17	3.0
$(NH_4)_6P_2Mo_{18}O_{62}$	0.11	$Mo_2C_{0.9}O_{0.78}P_{0.22}$	18	2.3
$(NH_4)_6P_2Mo_5O_{23}$	0.4	$Mo_2C_{0.34}O_{1.8}P_{0.82}$	30	1.8

The XRD results for the various materials synthesized are presented in Fig. 2. Comparison with a standard pattern from a powder diffraction file indicates that these compounds have the same structural type (fcc) as γ-Mo_2N (JCPDS 25-1366). Calculation yields a value of 0.4194(4) nm for the lattice parameter a, which is slightly greater than that for γ-Mo_2N ($a = 0.4163$ nm). Gouin *et al.* (29) have prepared two molybdenum oxynitrides: a high-surface-area compound (Mo_2N-A, $S_g = 120$ m^2 g^{-1}) and a low-surface-area compound (Mo_2N-B, $S_g = 20$ m^2 g^{-1}). The two materials differed in the temperature ramping rate and the final reaction temperature. The molybdenum oxynitride synthesized in this work compares well with the d-spacing and the relative intensities of the XRD patterns for Mo_2N-B. In agreement with Gouin *et al.* (29) we propose a face-centered cubic arrangement for our oxynitride materials. The highest intensity peak in the XRD pattern of the molybdenum oxynitride is that of the (111) plane while the usual XRD pattern of MoO_3-derived oxynitride (17, 29) shows the highest intensity peak for the (200) plane. This inversion is specific for the precursor used: ammonium heptamolybdate (8, 17). As observed in Table 1, the stoichiometry MoX_2 with X = N and O is confirmed (except that of P/Mo = 0.4) and can be obtained if the octahedral

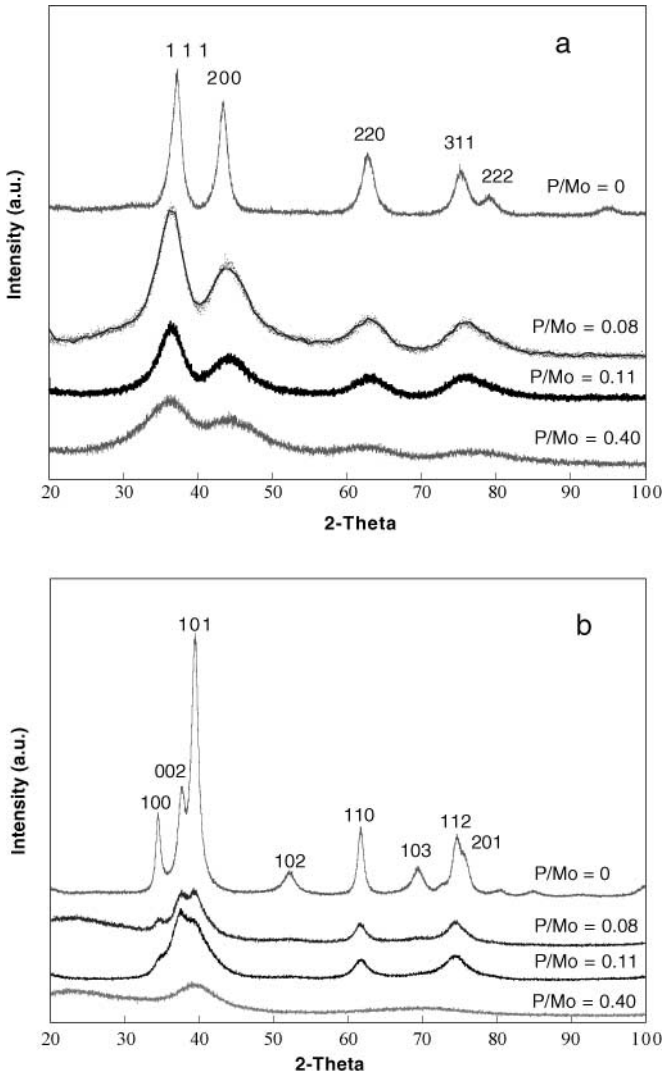

FIG. 2. X-ray diffraction patterns of molybdenum oxynitrides (a) and oxygen-modified carbides (b) prepared from different heteropolyanions.

voids of the network are occupied by molybdenum with a probability of around 0.5. Addition of phosphorus still maintains the fcc crystal structure of γ-Mo_2N but significant peak broadening is observed with increasing P/Mo content.

In the case of oxygen-modified molybdenum carbides the elemental analysis results (Table 1) show an amount of carbon slightly greater than required by the theoretical formula Mo_2C. The phosphorus-containing precursors lead to molybdenum carbides whose oxygen content rises as the P/Mo ratio increases. We present the chemical formulas of these materials as MoC_xO_y or $MoC_xO_yP_z$ and refer to them as oxygen-modified molybdenum carbides.

The XRD results for the various materials synthesized are presented in Fig. 2. Comparison with a standard pattern from a powder diffraction file indicates that the ammonium heptamolybdate-derived carbide is of the same structural type as β-Mo_2C (JCPDS 35-0787, $a = 0.3012$ and $c = 0.4735$ nm), a hexagonal close-packed structure. Calculations yield values of 0.3005(3) and 0.475(7) nm for the a and c lattice parameters, respectively, in agreement with those of the literature (27). The XRD patterns of the phosphorus-containing materials do not match exactly that of β-Mo_2C, as the broadening of the peaks prevent any comparison.

Evolution of the Specific Surface Area: Influence of the P/Mo Ratio

The surface areas and CO uptakes of the samples are reported in Table 2. Molybdenum oxynitrides derived from ammonium heptamolybdate have much greater specific surface areas than those prepared from phosphorus-containing precursors, in agreement with previous results (8, 17). The broadening of the XRD peaks together with the smaller specific surface areas suggest an agglomeration of particles for the P-molybdenum oxynitrides. The reduction of the P-containing precursors with NH_3 or CH_4/H_2 probably proceeds through amorphous glasses or molten intermediates.

Carbon monoxide is commonly used as a molecular probe to titrate the number of accessible surface metal atoms on molybdenum carbides or nitrides (2, 30). As shown in Table 2, the CO uptakes of the current samples range from high (434 μmol g^{-1}) to medium (231 μmol g^{-1}), assuming molecular adsorption and hence 1 : 1 stoichiometry between CO and the exposed adsorbing molybdenum atoms for molybdenum oxynitride. Normally, for metals the surface site density is about 1×10^{15} atoms per square centimeter (30). The values obtained (Table 2) in this study are in the range $0.16–0.30 \times 10^{15}$ atoms cm^{-2}, indicating that 16–30% of the surface molybdenum atoms are chemisorbing CO. For molybdenum oxynitrides these values are slightly smaller than those reported in the literature for different synthesis conditions (1, 31). Furthermore, it appears

TABLE 2

CO Chemisorption and Comparison of Turnover Rates (TOR) for Propene Hydrogenation over Molybdenum Oxynitrides and Oxygen-Modified Carbides

Precursor	P/Mo	CO chemisorption: Uptake (μmol g^{-1})	CO chemisorption: Site density ($\times 10^{15}$ cm^{-2})	TOR (s^{-1}): 353 K	TOR (s^{-1}): 383 K
Oxynitrides					
$Mo_2N_{2.7}O_{1.46}$	0	434	0.16	—	0.004
$Mo_2N_{2.82}O_{1.34}P_{0.2}$	0.08	231	0.30	0.093	—
$Mo_2N_{2.86}O_{0.82}P_{0.24}$	0.11	321	0.25	0.037	—
$Mo_2N_{1.08}O_{1.28}P_{0.82}$	0.4	—	—	—	—
Oxygen-modified carbides					
$Mo_2C_{1.46}O_{0.08}$	0	208	0.28	0.09[a]	
$Mo_2C_{0.9}O_{0.46}P_{0.16}$	0.08	156	0.53	0.15[a]	
$Mo_2C_{0.9}O_{0.78}P_{0.22}$	0.11	116	0.39	0.13[a]	
$Mo_2C_{0.34}O_{1.8}P_{0.82}$	0.4	234	0.47	0.12[a]	

[a] Performed at 250 K.

that the reduced amount of adsorbed CO for phosphorus-containing precursors is much greater than would be expected from the lower surface area and therefore reflects greatly reduced site densities. The specific surface area of the oxygen-modified molybdenum carbide compares well with those reported in the literature (8, 17, 26, 32, 33).

The measurements in this study were carried out on passivated and rereduced samples; for comparison we must take into account the final temperature and the CH_4/H_2 ratios. Elemental analysis gives for oxygen-modified carbide a C/Mo ratio of 0.7 (against 0.5 for Mo_2C), indicating an excess of carbon. The carburization profile (Fig. 1) indicates that the second CH_4 consumption peak is not associated with water production, but must be due to the deposition of excess free surface carbon in an amorphous, graphitic, or other aggregate form, as reflected by the elemental analysis.

As noted for oxynitrides, phosphorus leads to a lowering of the specific surface area, the reducing properties of phosphorus enhancing the metal site density. Of interest is the P/Mo = 0.4 material; this sample shows, in contrast to the oxynitride equivalent, the highest CO uptake and a moderate value of the specific surface area leading to a site density of 0.47×10^{15} atoms cm^{-2}. Nevertheless, the carbon content is low and the oxygen content high, in contrast with the other oxygen-modified molybdenum carbides. Carbides have higher site densities than do oxynitrides, but the active site density will be reflected by the TOR values.

XPS Analysis

X-ray photoelectron spectroscopy was used to obtain the surface composition of the catalyst together with information on the valence state and the chemical environment of Mo and P principally. The distribution of Mo oxidation states for molybdenum oxynitrides and oxygen-modified molybdenum carbides was estimated by decomposition of the Mo 3d spectra (Figs. 3 and 4, respectively). Curve fitting of the Mo 3d peaks was accomplished using linked

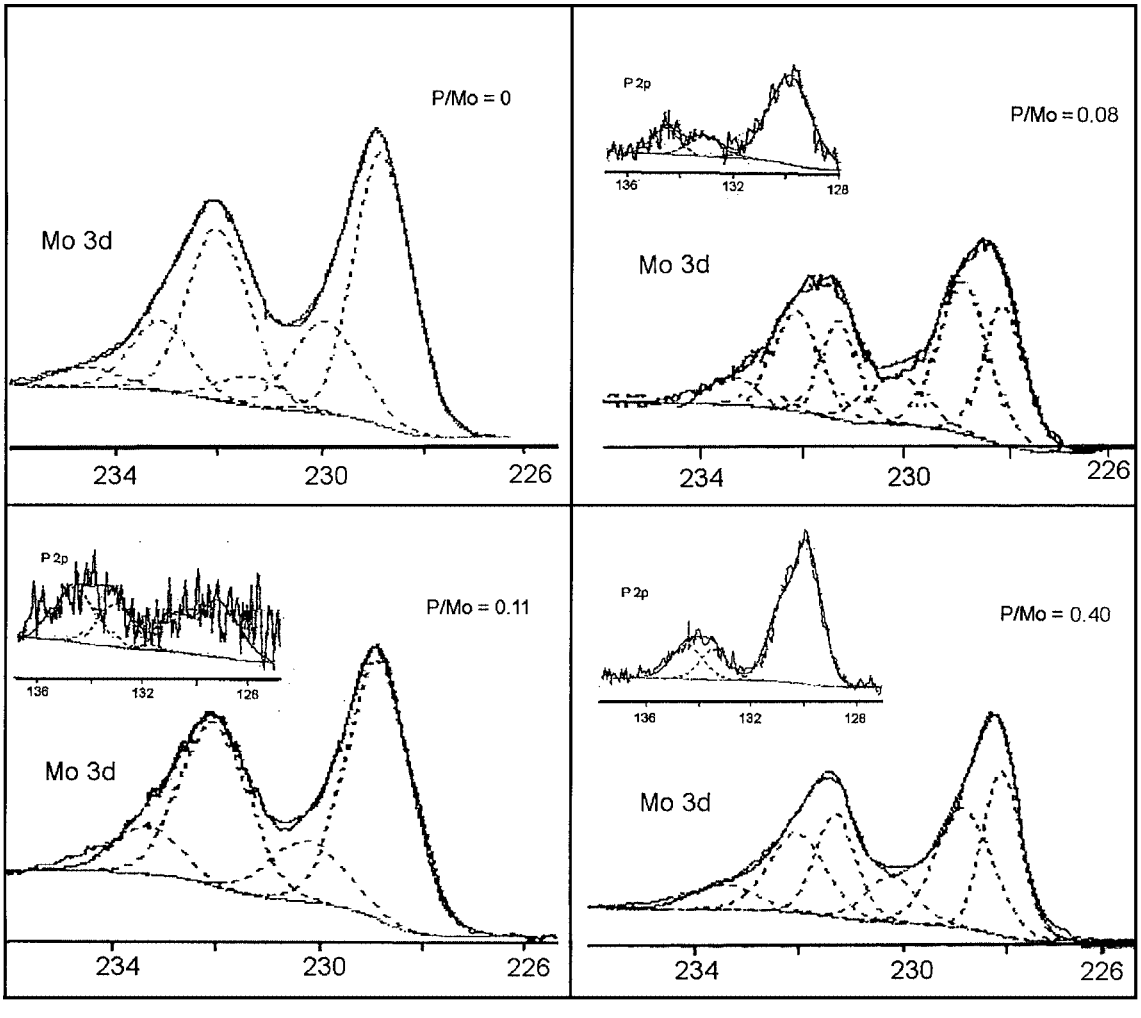

FIG. 3. Molybdenum oxynitride samples: decomposition of experimental XPS spectra at Mo 3d and P 2p (inset) levels for $Mo_2N_{2.7}O_{1.46}$ (P/Mo = 0) (a); $Mo_2N_{2.82}O_{1.34}P_{0.2}$ (P/Mo = 0.08) (b); $Mo_2N_{2.86}O_{0.82}P_{0.24}$ (P/Mo = 0.11) (c); and $Mo_2N_{1.08}O_{1.28}P_{0.82}$ (P/Mo = 0.4) (d).

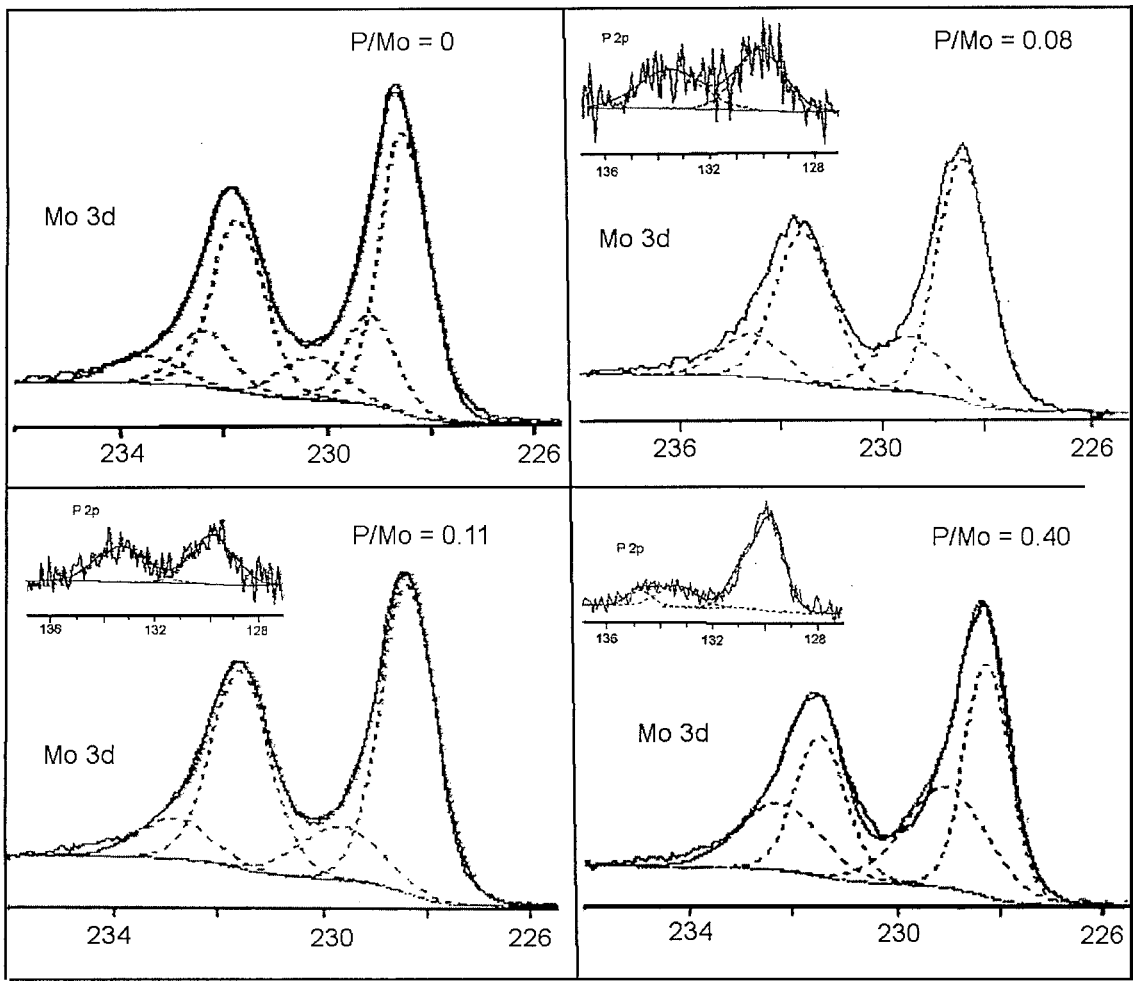

FIG. 4. Oxygen-modified molybdenum carbide samples: decomposition of experimental XPS spectra at Mo 3d and P 2p (inset) levels for $Mo_2C_{1.46}O_{0.08}$ (P/Mo = 0) (a); $Mo_2C_{0.9}O_{0.46}P_{0.16}$ (P/Mo = 0.08) (b); $Mo_2C_{0.9}O_{0.78}P_{0.22}$ (P/Mo = 0.11) (c); and $Mo_2C_{0.34}O_{1.8}P_{0.82}$ (P/Mo = 0.4) (d).

doublets ($Mo\,3d_{5/2}$–$Mo\,3d_{3/2}$) corresponding to two or three different molybdenum species with binding energies below 231.6 eV and higher than 227.9 eV. Table 3 summarizes the XPS results.

A species with a $Mo\,3d_{5/2}$ binding energy of about 229 eV was identified, midway between those assigned to Mo^{4+} (230 ± 0.2 eV) and Mo^0 (227.8 ± 0.2 eV) and close to that of Mo^{2+} (228.2 ± 0.2 eV) (34, 35). This binding energy has often been observed for molybdenum nitrides (35–37) and carbides (38).

The species associated with this binding energy has been denoted as $Mo^{\delta+}$ and in our materials is involved in Mo–N or Mo–C bonds. For the molybdenum oxynitrides approximately 45–65% of the total surface molybdenum was present as $Mo^{\delta+}$ while for the oxygen-modified molybdenum carbides it was 18–44%. XPS spectrum deconvolution for molybdenum oxynitrides led to an additional contribution of Mo^{4+} and a substantial contribution of Mo^0 for the two P-containing materials. The binding energy of 231.6 eV (P-free molybdenum oxynitride) was assigned to Mo^{5+} (34).

The N 1s spectra overlapped with the $Mo\,3p_{3/2}$ spectra in the range 390–410 eV. Therefore, the $Mo\,3p_{1/2}$ spectra were reconstructed and fitted from the distribution of the Mo 3d spectra while keeping the same intensity ratio for the Mo species peaks. For the decomposition of the $Mo\,3p_{3/2}$ signal, splitting energies of 17.5 eV and the appropriate intensity ratio were applied on the basis of the $Mo\,3p_{1/2}$ signal. To complete the experimental envelope the nitrogen component N 1s was then introduced. Curve fitting was then performed with the intensity ratios of Mo species fixed and the system was refined to test the validity of the model (37, 39, 40). The XPS N 1s binding energies are in the range 397.6–398.4 eV (Table 3), as reported for Mo–N bonds (36, 37, 41, 42).

For the oxygen-modified molybdenum carbides, the C 1s signal was fitted with three components centered at 284.6 eV (adventitious carbon), 283.3 eV (identified as

TABLE 3

X-Ray Photoelectron Spectroscopy Analysis of Molybdenum Oxynitrides and Oxygen-Modified Carbides with Different P/Mo Ratios

	O 1s		N 1s	P 2p			Mo $3d_{5/2}$			
Oxynitrides	Oxide		(Nitride)	P–Mo	P–(O, N)	P–(O, N)	Mo^0	$Mo^{\delta+}$	Mo^{4+}	Mo^{5+}
P/Mo										
0	530.6	532.5	398.4					229.0 (66%)	230.2 (26%)	231.6 (8%)
0.08	531.1	532.5	397.8	129.7 (59%)	133.0 (18%)	134.4 (23%)	228.1 (35%)	228.8 (47%)	230.1 (18%)	
0.11	530.9	532.6	397.6	129.1 (36%)	133.1 (26%)	134.5 (39%)		228.8 (80%)	230.2 (20%)	
0.40	531.2	533.1	398.0	129.7 (66%)	133.3 (19%)	134.3 (15%)	228.0 (41%)	228.7 (44%)	230.1 (15%)	
	O 1s		C 1s	P 2p			Mo $3d_{5/2}$			
Oxygen-modified carbides	Oxide		Carbide	P–Mo	P–(O, N)	P–(O, N)	Mo^0	MO^{5+}	Mo^{4+}	
P/Mo										
0	530.7		283.3	286.1				228.3 (54%)	229.1 (36%)	230.2 (10%)
0.08	531.0	532.8	283.3	285.9	129.9 (47%)	133.4 (53%)		228.3 (85%)	229.4 (15%)	
0.11	530.6	533.1	283.2	286.2	129.7 (46%)	133.1 (54%)		228.1 (82%)	229.5 (18%)	
0.40	531.2	533.1	283.3	286.1	129.4 (66%)	133.1 (11%)	134.5 (23%)	227.9 (56%)	228.7 (44%)	

Note. Binding energies (eV) and concentration (%) of Mo $3d_{5/2}$ species. The number in brackets represents the percentage area of the Mo or P species.

carbidic carbon involved in Mo–C bonds) (38, 43, 44), and a shoulder at about 286 eV corresponding to oxidized carbon entities (45).

The region of the O 1s spectra includes two peaks. It is generally accepted that peaks at about 530 eV are due to oxides and those at about 532 eV to adsorbed oxygen species such as O^-, OH^-, or H_2O (35).

A two-peak profile was observed for the P 2p signal. The first peak at higher binding energy can be decomposed into two components, indicating that there are two kinds of P species, corresponding to P–O or P–N bonds, as also reported by Li and Lee (8, 9, 17).

The other peak observed at about 130 eV was attributed to P bonded to Mo. A molybdenum phosphide was synthesized as reported (46) and comparison of the XRD pattern with that of MoP (47) established the similarity of the structure (phosphorus is trigonal prismatically, surrounded by molybdenum atoms). Curve fits of the Mo 3d and P 2p regions in the XPS spectrum reveal that about 25% of the surface region is oxidized to phosphate (binding energy, 133.6 eV) and 75% is in the reduced phosphide state (binding energy, 129.2 eV). The oxidation is due to air exposure of the sample before XPS analysis. A binding energy of 229.9 eV is reported for the Mo 3d region attributed to Mo^{4+}. For comparison, we estimate that in P-containing molybdenum oxynitrides and *oxygen-modified carbides* about 50% of the phosphorus species (Table 3) concern phosphide.

As observed by XPS, the P-containing molybdenum oxynitrides present a higher concentration of lower oxidation states of molybdenum ($Mo^0 + Mo^{\delta+}$), accounting for about 80% of the molybdenum species. In the P-containing oxygen-modified molybdenum carbides all the molybdenum is in low oxidation states, with about 80% Mo^0 (for P/Mo = 0.08 and 0.11). It can be seen that for both series of materials the reducibility of the molybdenum species increases when phosphorus is present.

The surface composition of molybdenum oxynitrides and oxygen-modified carbides as determined by XPS is reported in Table 4. For all materials the phosphorus content increases with the P/Mo ratio; this is generally

TABLE 4

Surface Composition (Formula) as Determined by XPS for Molybdenum Oxynitrides and Oxygen-Modified Carbides

Oxynitride	Oxygen-modified carbide
$Mo_2N_{0.66}O_{1.66}$	$Mo_2C_{1.96}O_{0.22}$
$Mo_2N_{1.28}O_{1.62}P_{0.86}$	$Mo_2C_{1.52}O_{1.6}P_{0.4}$
$Mo_2N_{1.9}O_{1.82}P_{0.66}$	$Mo_2C_{1.18}O_{1.36}P_{0.5}$
$Mo_2N_{0.6}O_{1.46}\ P_{0.82}$	$Mo_2C_{1.06}O_{1.4}P_{0.9}$

associated with a segregation of oxygen atoms, which move toward the surface. Therefore, it is very likely that oxygen is more associated with phosphorus at the surface of the catalyst rather than with the metal, which would explain the lower oxidation states for Mo (higher metallic character).

Hydrogenation Properties

Propene hydrogenation was selected as a molecular probe reaction to evaluate the role of phosphorus on the hydrogenation activity of our materials. The specific rate (micromoles per second per gram of catalyst) could be deduced from the initial conversion; assuming that active sites are titrated by CO, a propene hydrogenation turnover rate (TOR) could therefore be easily obtained.

It is observed that the P-containing catalysts have higher TOR than those without phosphorus. The effect of phosphorus is more evident for oxynitrides than for oxygen-modified carbides; it should be noted that no reaction occurred at 353 K with phosphorus-free molybdenum oxynitride (hydrogenation must be performed at 383 K for this material). According to the TOR results the P-molybdenum oxygen-modified carbides have substantially higher hydrogenation capacity than the related oxynitrides. The former materials were active at 250 K, whereas to obtain similar activity with P-containing molybdenum oxynitrides, hydrogenation must be conducted at 353 K.

Consequently, from the XPS and TOR results it can be deduced that the hydrogenation character of molybdenum oxynitrides is strongly linked to the presence of phosphorus, which increases the metallic character of the molybdenum. Phosphorus, in addition to increasing the density of metallic sites, is capable of strengthening the active sites, as indicated by the value of the TOR. Furthermore, a surface P-enrichment creating molybdenum phosphides contributes to an increase in the rate of hydrogenation reactions, as reported earlier (47–49). Little effect is observed on the oxygen-modified carbides, which are already strongly metallic; surface molybdenum phosphides probably contribute to an enhancement of the hydrogenation activity.

An interesting comparison can be drawn with propene hydrogenation over P-containing tungsten oxynitrides at 353 K (10). The TOR are about 10 times higher than those of P-doped molybdenum oxynitrides. TOR values for P-doped oxygen-modified molybdenum carbides at 250 K are equivalent to those for P-doped tungsten oxynitrides at the higher temperature. Therefore these results lead to the following ranking: P–Mo oxygen-modified carbides > P–W–oxynitrides > P–Mo–oxynitrides.

CONCLUSION

New P-containing molybdenum oxynitrides and oxygen-modified carbides have been synthesized from various heteropolyanion precursors and characterized by chemical analysis, XRD, XPS, and chemisorption.

This work shows that the presence of phosphorus promotes the reduction of molybdenum; the amount of (Mo^0 + $Mo^{\delta+}$) and consequently the site density increase. The XPS data show that phosphorus has two types of environments: the first surrounded by molybdenum and the second surrounded by oxygen, nitrogen, or carbon. The hydrogenation function depends on two parameters: the number and the strength of the active sites. This study reveals that phosphorus has an effect on both; in the case of oxynitrides both factors are increased, whereas for the oxygen-modified carbides, which are already quite metallic, the number of sites rises but the strength is little modified.

As the TOR of propene hydrogenation over P-containing oxynitrides is much higher than for a catalyst without P, its activity has to be measured at 30 K lower than for the catalyst without phosphorus. The results show that the P–oxygen-modified carbides are still more active in hydrogenation than the P–oxynitrides. The TOR value for a carbide is much the same with or without phosphorus.

ACKNOWLEDGMENTS

P. Pérez-Romo is grateful to the Consejo Nacional de Ciencia y Tecnologia (CONACyT) for financial support. The help of M. Leclerc and P. Bargiela with the XPS measurements is greatly appreciated. We thank Dr. J. S. Lomas for constructive discussions and for correcting the manuscript.

REFERENCES

1. Volpe, L., and Boudart, M., *J. Solid State Chem*. **59**, 332 (1985).
2. Oyama, S. T., Schlatter, J. C., Metcalfe, J. E., and Lambert, J. M., *Ind. Eng. Chem. Res.* **27**, 1639 (1988).
3. Levy, R. B., and Boudart, M., *Science* **181**, 457 (1973).
4. Chen, J. G., *Chem. Rev.* **96**, 1477 (1996).
5. "The Chemistry of Transition Metal Carbides and Nitrides." S. T., Oyama, Ed., Blackie, London, 1996.
6. van Veen, J. A. R., Colijn, H. A., Hendriks, P., and van Welsenes, A. J., *Fuel Process. Technol.* **35**, 137 (1993).
7. Eijsbout, S., van Gestel, J. N. M., van Veen, J. A. R., de Beer, V. H. J., and Prins, R., *J. Catal.* **131**, 412 (1991).
8. Li, S., and Lee, J. S., *J. Catal.* **178**, 119 (1998).
9. Li, S., and Lee, J. S., *J. Catal.* **173**, 134 (1998).
10. Pérez-Romo, P., Potvin, C., Manoli, J.-M., and Djéga-Mariadassou, G., *J. Catal.* **205**, 191 (2002).
11. Sellem, S., Potvin, C., Manoli, J.-M., Contant, R., and Djéga-Mariadassou, G., *J. Chem. Soc. Chem. Commun.* 359 (1995).
12. Pérez-Romo, P., Doctoral thesis. Université Pierre et Marie Curie, Paris, 1999.
13. Dhandapani, B., Ramanathan, S., Yu, C. C., Fruhberger, B., Chen, J. G., and Oyama, S. T., *J. Catal.* **176**, 61 (1998).
14. Da Costa, P., Potvin, C., Manoli, J.-M., Breysse, M., and Djéga-Mariadassou, G., *Catal. Lett.* **72**, 91 (2001).
15. Da Costa, P., Potvin, C., Manoli, J.-M., Lemberton, J.-L., Pérot, G., and Djéga-Mariadassou, G., *J. Mol. Catal*., in press.
16. Da Costa, P., Doctoral thesis. Université Pierre et Marie Curie, Paris, 2000.
17. Li, S., and Lee, J. S., *J. Catal.* **162**, 76 (1996).

18. Scherrer, P., *Nachr. Ges. Wiss. Göttingen* **26**, 198 (1918).
19. Seah, M. P., *in* "Practical Surface Analysis by Auger and X-ray Photoelectron Spectroscopy" (D. Briggs and M. P. Seah, Eds.), Vol. 1, Chap. 5, pp. 225–226. Wiley, New York, 1990.
20. Burwell, R. L., *Langmuir* **2**, 2 (1986).
21. Germain, J. E., and Maurel, R., *C. R. Acad. Sci.* **247**, 1854 (1958).
22. Jaggers, C. H., Michaels, J. N., and Stacy, A. M., *Chem. Mater.* **2**, 150 (1990).
23. Choi, J.-G., Curl, R. L., and Thompson, L. T., *J. Catal.* **146**, 218 (1994).
24. Bécue, T., Doctoral thesis. Université Pierre et Marie Curie, Paris, 1996.
25. Gouin, X., Doctoral thesis. Université de Rennes, 1993.
26. Lee, J. S., Oyama, S. T., and Boudart, M., *J. Catal.* **106**, 125 (1987).
27. Choi, J.-S., Bugli, G., and Djéga-Mariadassou, G., *J. Catal.* **193**, 238 (2000).
28. Li, S., Kim, W. B., and Lee, J. S., *Chem. Mater.* **10**, 1853 (1998).
29. Gouin, X., Marchand, R., L'Haridon, P., and Laurent, Y., *J. Solid State Chem.* **109**, 175 (1994).
30. Lee, J. S., Lee, K. H., and Lee, J. Y., *J. Phys. Chem.* **96**, 362 (1992).
31. Ranhotra, G. S., Haddix, G. W., Bell, A. T., and Reimer, J. A., *J. Catal.* **108**, 24 (1987).
32. Ramanathan, S., and Oyama, S. T., *J. Phys. Chem.* **99**, 16365 (1995).
33. Dhandapani, B., St. Clair, T. P., and Oyama, S. T., *Applied Catal. A* **168**, 219 (1998).
34. Quincy, R. B., Houalla, M., Proctor, A., and Hercules, D. M., *J. Phys. Chem.* **94**, 1520 (1990).
35. Choi, J.-G., and Thompson, L. T., *Appl. Surf. Sci.* **93**, 143 (1996).
36. Choi, J.-G., Brenner, J. R., Colling, C. W., Demczyk, J. L., Dunning, J. L., and Thompson, L. T., *Catal. Today* **15**, 201 (1992).
37. Bécue, T., Manoli, J.-M., Potvin, C., Delamar, M., and Djéga-Mariadassou, G., *J. Phys. Chem. B* **101**, 6429 (1997).
38. Ledoux, M. J., Pham-Huu, C., Guille, J., and Dunlop, H., *J. Catal.* **134**, 383 (1992).
39. Nagai, M., Irisawa, A., and Omi, S., *J. Phys. Chem. B* **102**, 7619 (1998).
40. Hada, K., Nagai, M., and Omi, S., *J. Phys. Chem. B* **104**, 2090 (2000).
41. Ozkan, U. S., Zhang, L., and Clark, P. A., *J. Catal.* **172**, 294 (1997).
42. Choi, J.-G., Choi, D., and Thompson, L. T., *Appl. Surf. Sci.* **108**, 103 (1997).
43. St. Clair, T. P., Oyama, S. T., Cox, D. F., Otani, S., Ishizawa, Y., Lo, R.-I., Fukui, K., and Iwasawa, Y., *Surf. Sci.* **426**, 187 (1999).
44. Ramqvist, L., Hamrin, K., Johansson, G., Fahlman, A., and Nordling, C., *J. Phys. Chem. Solids* **30**, 1835 (1969).
45. Paal, Z., Xu, X. L., Paal-Lukacs, J., Vogel, W., Muhler, M., and Schogl, R., *J. Catal.* **152**, 252 (1995).
46. Rundqvist, S., and Lundström, T., *Acta Chem. Scand.* **17**, 37 (1963).
47. Stinner, C., Prins, R., and Weber, T., *J. Catal.* **191**, 438 (2000).
48. Li, W., Dhandapani, B., and Oyama, S. T., *Chem. Lett.* 207 (1998).
49. Stinner, C., Prins, R., and Weber, T., *J. Catal.* **202**, 187 (2001).